A virtual real-time hybrid simulation framework to study mooring dynamics of deep-water wave energy converters (WECs)

Conference Paper · August 2025

CITATIONS
0

READS
28

8 authors, including:

Elaine Liu
Stanford University
2 PUBLICATIONS **0** CITATIONS
SEE PROFILE

Abilyn McConnell
Oregon State University
1 PUBLICATION **0** CITATIONS
SEE PROFILE

Yun Ni
Stanford University
3 PUBLICATIONS **0** CITATIONS
SEE PROFILE

Akiri Seki
Stanford University
11 PUBLICATIONS **22** CITATIONS
SEE PROFILE

UMERC+OREC
2025 Conference

12-14 August | Corvallis, OR USA

A virtual real-time hybrid simulation framework to study mooring dynamics of deep-water wave energy converters (WECs)

Elaine Liu[1a], Abilyn Mcconnell[b], Bret Bosma[b], Yun Ni[a], Akiri Seki[a], Andreas Schellenberg[c], Bryson Robertson[b], Barbara Simpson[a]

[a]*Stanford University, Stanford, CA 94305, US*
[b]*Oregon State University, Corvallis, OR 97331, US*
[c]*Maffei Structural Engineering, San Francisco, CA 94111, US*

Abstract

Wave energy has enormous potential as a renewable energy resource, but characterizing device and mooring line behavior in deep-water regimes is difficult due to the size constraints in traditional laboratory testing. A real-time hybrid simulation (RTHS) framework is proposed to emulate deep-water mooring lines in reduced-scale experiments. RTHS couples physical experiments with numerical models to virtually deepen existing hydrodynamic facilities. In the proposed framework, a small-scale wave energy converter (Sub-WEC) will be physically tested in the Large Wave Flume at Oregon State University. The mooring line will be numerically simulated using MoorDyn, which will send commands to a motor to emulate tensions on the line, representative of the device placed in deep-water regimes. Sensor measurements of Sub-WEC will then serve as inputs to update the next iterative state of the numerical model. To validate the feasibility of the hybrid approach prior to flume testing, the study herein examines a virtual-RTHS framework using numerical proxies to virtually rehearse the communication and data exchange between the numerical and physical sub-assemblies. The communication architecture uses a modular, three-loop architecture for improved synchronization. A numerical model represents the actuation motor, derived from governing equations of motion and system identification. An estimation procedure of the parameters in the equations of motion as well as discrepancies

[1] ∗ Corresponding author..
E-mail address: ejl2401@stanford.edu

in the numerical model and experimental data are discussed. This virtual framework provides a means of testing the communication architecture prior to flume testing, with future work involving fine tuning the actuator model to obtain a more realistic virtual simulation.

Keywords: wave energy converters; virtual real-time hybrid simulation; deep-water mooring; system identification

1 Introduction

Offshore wave energy, particularly in deep waters, has tremendous potential to contribute to the clean energy transition due to its high predictability, consistency and energy density [1]. However, validating deep-water wave energy converters in marine operating environments is challenging due to financial constraints and risk factors in open-water testing [2]. Moreover, traditional laboratory-based testing methods, such as wave basin or flume testing, do not have the depths to test devices along with the full-length of their mooring lines at a reasonable scale. These limitations emphasize a need for alternative approaches to test and validate deep-water devices.

Real-time hybrid simulations (RTHS) are a promising approach to enable enhanced testing of deep-water devices and their mooring lines in the maritime industry [3, 4]. Originating in earthquake engineering, RTHS is an experimental testing technique that combines physical modeling informed by a numerical model [5]. When applied to experiments of WECs with deep-water mooring lines, a physical floating structure experiencing wave loading is studied in a hydrodynamic facility, while actuators impose forces onto the floating structure to represent contributions from a numerically simulated mooring line extending to greater depths. Sensors on the floater then measure positional information to update the next iterative state of the numerical mooring model, completing one timestep of the hybrid simulation. Here, the numerical mooring system can virtually extend the depth of a wave facility, enhancing existing laboratory capabilities [6, 7].

Various numerical studies and virtual real-time hybrid simulations have been conducted to assess the feasibility of a hybrid test prior to wave basin/flume testing [8, 9]. In a virtual real-time hybrid simulation (virtual-RTHS), the physical sub-assembly and actuation system are replaced with numerical proxies, allowing for early evaluation of the hybrid framework in a virtual environment [10]. However, much of the prior work in virtual real-time simulations rely on application-specific architectures and do not explore modular frameworks needed for testing offshore hybrid simulations, particularly for ensuring minimal transmission delay and timing synchronization between the physical and numerical sub-assemblies.

The research herein demonstrates a virtual-RTHS setup that implements a modular, three-loop hardware architecture [11] to examine the response of a deep-water wave energy converter (WEC) subjected to wave loading. The system was partitioned into two sub-assemblies: a "physical" subassembly consisting of the wave loading and lab-scale specimen for the device, as well as a full-scale numerical subassembly representing the mooring line computed using MoorDyn [12]. The wave energy converter modeling software WEC-Sim [13] was used to virtually simulate the lab-scale specimen, while numerical proxies were developed to model the actuation system, thereby realizing the entire "physical" sub-assembly. The virtual framework will provide a means to rehearse a complete RTHS experiment prior to tank testing, allowing for flexibility and rapid testing iterations.

2 Proposed RTHS Framework

The device of interest is Sub-WEC, a simple, cylindrical wave energy converter that can be moored in a single tether configuration [14]. To construct the hybrid model, the system is partitioned into physical and numerical sub-assemblies, as shown in Figure 1(a). The physical sub-assembly contains the scaled test specimen in the wave flume, which consists of a 1:12-scale Sub-WEC (i.e. $\lambda_L = 12$) and physical wave loading conditions. The numerical sub-assembly consists of the numerically simulated full-scale mooring line, modeled using the mooring dynamics solver MoorDyn [12]. MoorDyn is a computationally efficient, lumped-mass mooring line dynamics model that can be coupled with WEC-Sim to analyze structural and mooring interactions [15].

Figure 1(b) shows a schematic of the RTHS experiment. The sub-assemblies interface at the fairlead, where the mooring line connects to Sub-WEC; in this fashion, the entire mooring line is numerical. At a given timestep, Sub-WEC's six degree-of-freedom position and velocity measurements, denoted as $\boldsymbol{x}$ and $\dot{\boldsymbol{x}}$, are sent to MoorDyn to compute the corresponding six degree-of-freedom mooring forces $\boldsymbol{f}$ acting on the body. The magnitude of the

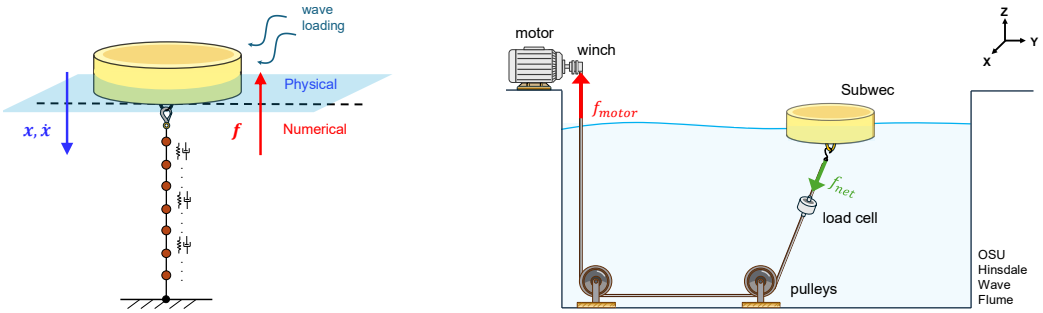

Figure 1: (a) Partitioning in the RTHS experiment. $\boldsymbol{x}$ and $\dot{\boldsymbol{x}}$ denote the six degree-of-freedom position and velocity measurements of SubWEC, while $\boldsymbol{f}$ denote the six degree-of-freedom mooring forces on the body; (b) Physical experimental setup showing actuation system. f_{net} denotes the magnitude of the force vector computed with MoorDyn, while f_{motor} denotes the commanded force to the motor to achieve f_{net} at the load cell.

translational mooring forces f_{net} are then imposed on the physical sub-assembly via commands to a winched motor, f_{motor}, mounted to the side of the wave flume. For simplicity, the research herein considers the single degree-of-freedom magnitude of the total mooring force. Thus, the actuation line is routed through a series of pulleys (fixed at the bottom of the wave basin) to ensure that tensions are primarily applied in the vertical heave direction (Figure 1(b)). Note that due to significant pretension in the system, it is assumed that SubWEC will mainly displace in the heave direction, with minimal displacements in the x-direction. Because of this, any angular deviation of force application from wave loading is considered negligible for our application. In the proposed experiment, the actuation line is made of Dyneema, a strong fiber commonly used in offshore applications for mooring lines and subsea tethers for its low stretch and high strength [16]. A Sensing Systems submersible load cell with a 4000 N rated capacity is also placed on the actuation line to measure in-line tensions [17]. The actuation motor herein uses an Akiribis B-series iron core rotary motor [18], an Altra Industrial Motion E-Brake, and a Beckhoff control system. A 0.3 m diameter pulley was attached to connect the actuation line.

3 Virtual-RTHS Implementation

A virtual-RTHS was developed to simulate the hybrid simulation prior to wave flume testing. The virtual system herein implements a modified modular software scheme via a three-loop architecture [19] consisting of two independent machines, namely a simulation “host" machine and a real-time “target" machine (See Fig. 2). By parallelizing and separating tasks across different processors, increased execution speeds and modularity of individual subsystems can be achieved [11]. Note that the typical three-loop architecture employs three machines via a third controller machine, but was simplified here into two machines by housing the controller algorithms into the "target" machine. The host machine uses Intel’s Core i9-14900KS for its CPU and the Windows operating system. The target machine, a Speedgoat, facilitates real-time data exchange to realize the full real-time hybrid model.

The “host" machine houses the numerical model, MoorDyn, as well as a middleware software, OpenFresco [19]. OpenFresco is a software package that serves to facilitate data exchange between numerical, finite-element models with control and data acquisition systems in physical testing facilities. In the virtual loop, the target machine houses WEC-Sim to simulate output from data acquisition in a laboratory, as well as facilitates time synchronization between the two machines. The machines communicate through fiber optic cables using SCRAMNetGT, a shared memory network, for its high-speed, ultra-low-latency transfer of data.

In a given timestep, WEC-Sim solves its governing equations of motion every $\Delta t_{con} = 0.002\ s$ to output Sub-WEC’s six degree-of-freedom position and velocity $(\boldsymbol{x}, \dot{\boldsymbol{x}})$, representative of Sub-WEC’s motion measurements obtained from a motion tracking camera in a wave flume test. As needed to account for potential noise in the signal readings, moving average and low pass filters are subsequently applied to smooth the input motions. Since typical hardware sensors operate at a deterministic time-step Δt_{con}, while numerical solvers operate at a non-deterministic time-step Δt_{int} ($\Delta t_{con} < \Delta t_{int}$), a timing algorithm is necessary to provide a buffer time, allowing the numerical model sufficient time to compute the next mooring forces. The time synchronization algorithm uses an internal counter N that accumulates to $N = 5$, thereby introducing a rate-transition timestep Δt_{sim}, before sending a signal to the host computer. For

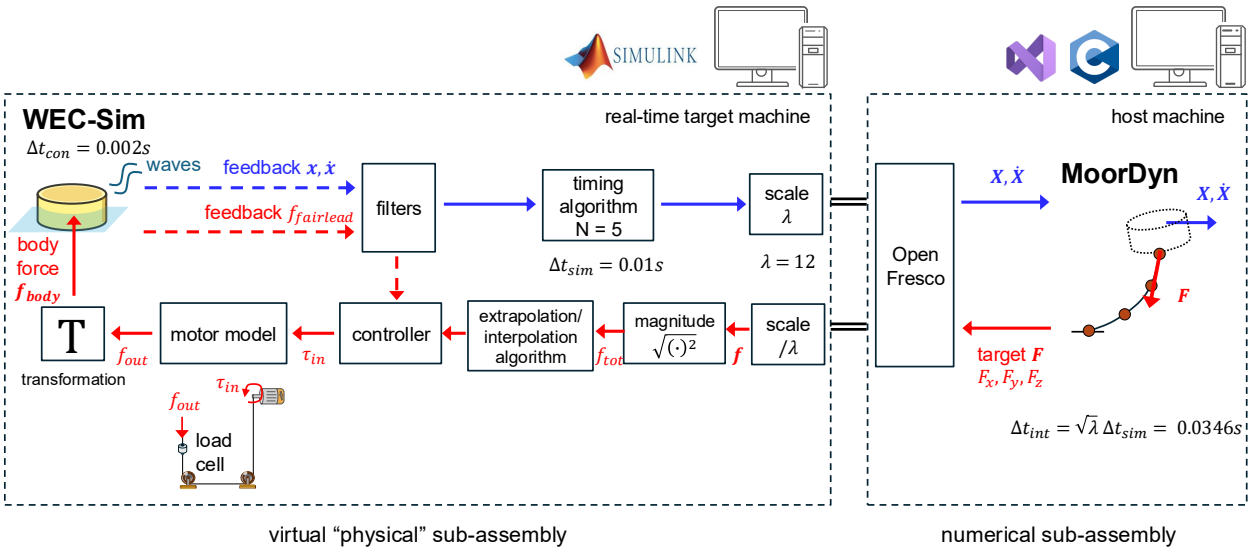

Figure 2: Schematic of virtual hybrid simulation communications architecture. $\boldsymbol{x}, \dot{\boldsymbol{x}}$ and $\boldsymbol{X}, \dot{\boldsymbol{X}}$ = feedback positions and velocities of lab-scale and full-scale SubWEC, respectively; $\boldsymbol{f}, \boldsymbol{F}$ = three degree-of-freedom lab-scale and full-scale mooring forces computed using MoorDyn, respectively; f_{tot} = magnitude of the lab-scale mooring force vector; τ_{in} = input command torque at the motor; f_{out} = force in the cable as read by the load cell; $\boldsymbol{f_{body}}$ = resultant six degree-of-freedom forces on SubWEC's center of mass; $f_{fairlead}$ = feedback magnitude of the force at the fairlead.

additional resolution and improved synchronization, the controller timestep is further upsampled by a factor of 5. The use of three separate time-steps constitute the three-loop architecture, where

$$\Delta t_{int} = \sqrt{\lambda_L}\,\Delta t_{sim} = \sqrt{\lambda_L}\,N\Delta t_{con} \tag{1}$$

After the timing algorithm, the signal is then scaled to full-scale according to Froude's similitude law to preserve length and time ratios, maintaining the small-scale open-channel flow of the experiment. These full-scale displacements and velocities $(\boldsymbol{X}, \dot{\boldsymbol{X}})$ are passed to the host machine, where OpenFresco facilitates data exchange between data acquisition machine and the numerical model. OpenFresco sends the full-scale data to the numerical model MoorDyn, which solves its own governing equations of motion at $\Delta t_{int} = 0.0346$ s and returns full-scale target fairlead forces $\boldsymbol{F}$ in three-degrees-of-freedom to the target machine. The forces are then scaled down using Froude similitude to obtain lab-scale mooring forces, $\boldsymbol{f}$. The magnitude of the three translational forces, f_{tot}, are then computed to be applied on the physical specimen.

Since WEC-Sim operates on a deterministic time-step of Δt_{con}, an extrapolation-interpolation algorithm is employed to continuously predict and send forces to be applied on the WEC-Sim body. Once the fairlead force is finished calculating via the numerical model, the extrapolation-interpolation algorithm corrects for force inputs to achieve the target force at the end of the numerical time-step Δt_{int}. Note, Δt_{con} is assumed to be small enough such that both the virtual proxy and numerical sub-assembly are synchronized without iterations.

To ensure accuracy of force being applied, a controller algorithm for the motor can be implemented with a feedback force term $f_{fairlead}$ from WEC-Sim, where $f_{fairlead}$ is the magnitude of the current fairlead force vector. Since the motor typically operates in torque-control, the force at the motor is scaled with the radius of the pulley to obtain command torque, τ_{in}. This command torque τ_{in} is input into a numerical proxy of the motor and cable system to obtain the resulting force at the end of the cable f_{out}, with derivation of the model explained in Section 3.1. To ensure compatibility with WEC-Sim, the applied fairlead force is then transformed into six degree-of-freedom body forces $\boldsymbol{f_{body}}$ to complete the current timestep.

3.1 Motor Model Derivation

To construct a numerical model of the motor and cable system, a simplified experimental setup was developed at the Wallace Energy Systems and Renewables Facility at Oregon State University. The actuation motor to be used in the

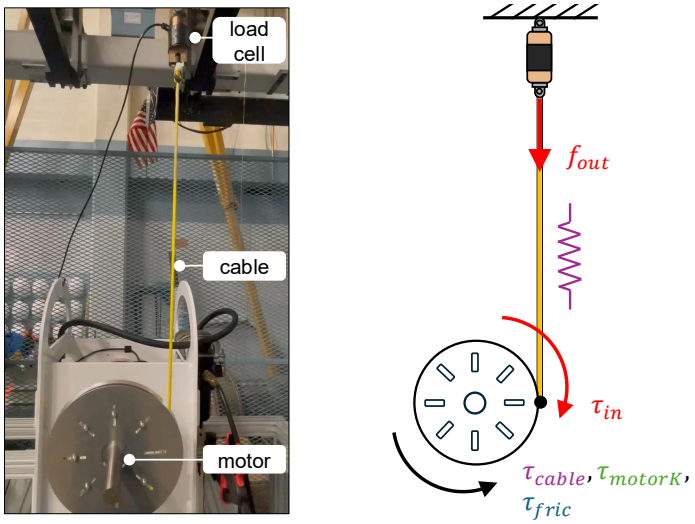

Figure 3: (a) Experimental setup of the motor; (b) Schematic for derivation of the numerical model

flume test was mounted to the base of the Ocean Wave Linear Test Bed (LTB), with a pulley connected to its shaft. The motor operated in torque control, receiving input torque commands τ_{in} to apply force to an actuation line that is fixed to the carriage on the LTB. A load cell at the top of the rail measured corresponding force readings in the cable f_{out}.

To model the dynamic behavior of the system, Newton's second law for rotation was used to derive a second order differential equation relating the system's inertia I to the net torque τ experienced.

$$I\alpha = \sum \tau \tag{2}$$

At a given time, the system receives command input torque τ_{in} and experiences resistive torques opposing the motion via the cable τ_{cable}, the motor's internal stiffness τ_{motorK}, and friction $\tau_{friction}$. The cable can be modeled as a spring element k_{cable}, where the spring constant relates to F_{cable} via deformation of the cable x and displacement of the LTB z. Similarly, the motor's resistance to rotation can also be modeled as a spring element k_{motor}, which relates to the resistive force in the motor F_{motorK} to the rotation of the motor, θ. Friction $\tau_{friction}$ can also be decoupled into constant and velocity-dependent damping terms, notably τ_c for constant Coulomb friction and b for the viscous damping friction coefficient. Note that the constant Coulomb term opposes the motion of the object, and thus depends on the sign of the motor velocity term, i.e. $sgn(\dot{\theta})$.

From the above, the following equation can be derived to obtain a numerical model that describes the rotational dynamics of the motor:

$$\begin{aligned} I\ddot{\theta} &= \tau_{in} - \tau_{cable} - \tau_{motorK} - \tau_{friction} \\ &= \tau_{in} - r \cdot F_{cable} - r \cdot F_{motorK} - (\tau_c \cdot sgn(\dot{\theta}) + b\dot{\theta}) \\ &= \tau_{in} - r \cdot k_{cable}(z + x) - r \cdot k_{motor}\theta - (\tau_c \cdot sgn(\dot{\theta}) + b\dot{\theta}) \end{aligned} \tag{3}$$

where I describes the total inertia of the motor and drum; θ describes the rotation of the motor; r is the radius of the drum; x and z is the vertical displacement of the cable and LTB, respectively.

In the above experimental setup, the carriage on the LTB is fixed and stationary, so displacements of the LTB would be 0 (i.e. $z = 0$). Thus, the above equation is simplified into:

$$I\ddot{\theta} = \tau_{in} - r \cdot k_{cable}x - r \cdot k_{motor}\theta - (\tau_c \cdot sgn(\dot{\theta}) + b\dot{\theta}) \tag{4}$$

The parameter I can be obtained from the sum of rotor inertia based on the motor's datasheet and pulley inertia as estimated in CAD. k_{cable} can be estimated using experimental data from linear torque ramp tests. The deformation of the cable is assumed to be related to the rotation of the motor, as $x = r \cdot \theta$, and incorporates pretension in the system.

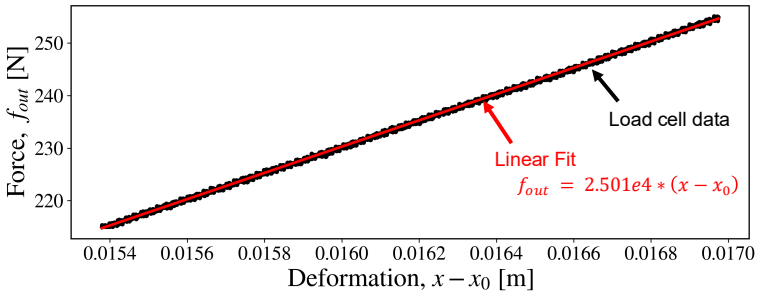

Figure 4: Figure of force-deformation relationship in the cable after applying pretension. Experimental data from the load cell reading is shown in black while the approximated linear fit is shown in red.

4 Results

To estimate the cable stiffness term, a linear ramp torque of 30 Nm was applied at the motor over a duration of 60 s to measure the corresponding force in the cable , f_{out}, against displacement of the cable, x. Since pretension is applied in the system, a linear stiffness model was implemented for only the region after applying pretension [20]. Using a linear fit, the experimental data from the load cell can be best approximated as the line $f_{out} = 2.501e4 \cdot (x - x_0)$. The root mean square error (RMSE) between the linear fit and experimental data was found to be 0.271 N.

To estimate the other parameters (i.e., friction), the second-order differential equation (Eqn 4) is reduced to a first-order system of differential equations and simulated across time. Using the Nonlinear Grey-Box Model under Matlab's System Identification Toolbox[2], the coefficients of the differential equations are estimated based on nonlinear least-squares optimization by fitting the model to the experimental data. To provide an initial estimate of the parameters in the model, a grid search was performed with a wide range of parameters to compute the associated RMSE against the validation data. The set of parameters that yielded the lowest RMSE created the initial guess. Following this, new estimation bounds of ±20% of these initial values were created to fine tune precise values using Matlab's System Identification Toolbox. This process repeated until the final values converged, and the stiffness of the cable was within reasonable range given preliminary estimates from the linear ramp tests. It should be noted that the stiffness measured during dynamic loading is expected to be higher than the static loading case [21]. The input to the model is the input torque τ_{in} with the numerical estimate of the force at the load cell, f_{pred}, compared against the experimental data output f_{out}. Note that the command input torque can be transformed to input command force f_{in} via $f_{in} = \tau_{in}/r$.

Multisine excitation signals spanning 0.2-1.25 Hz in frequency and 24-28 Nm in amplitude were input into the motor to assess system behavior across the operating range of frequencies. Each signal included three distinct phase realizations and three repeating periods to enhance the signal-to-noise ratio. The RMSE between the numerical model estimates and the actual load cell reading is 1.55 N, with a normalized L2 error of 0.73%. A sample time trajectory is provided to compare the numerical estimate against the input command force and output experimental load cell readings (see Fig.5).

The parameter estimates of the numerical model are presented in the table below. The initial guess of the total inertia of the motor and drum were obtained based on specifications from the datasheet and estimates from CAD, respectively.

Table 1: Summary of parameters estimated through system identification

Parameter	**Value**	**Units**
Total inertia I	0.0403	kg m^2
Viscous damping coefficient b	20.033	Nms/rad
Coulomb friction τ_c	0.401	Nm
Cable effective stiffness k_{cable}	369282.43	N/m
Motor rotational stiffness k_{motor}	0.974	N/rad
Pulley radius r	0.1143	m

[2]https://www.mathworks.com/help/ident/ug/estimating-nonlinear-grey-box-models.html

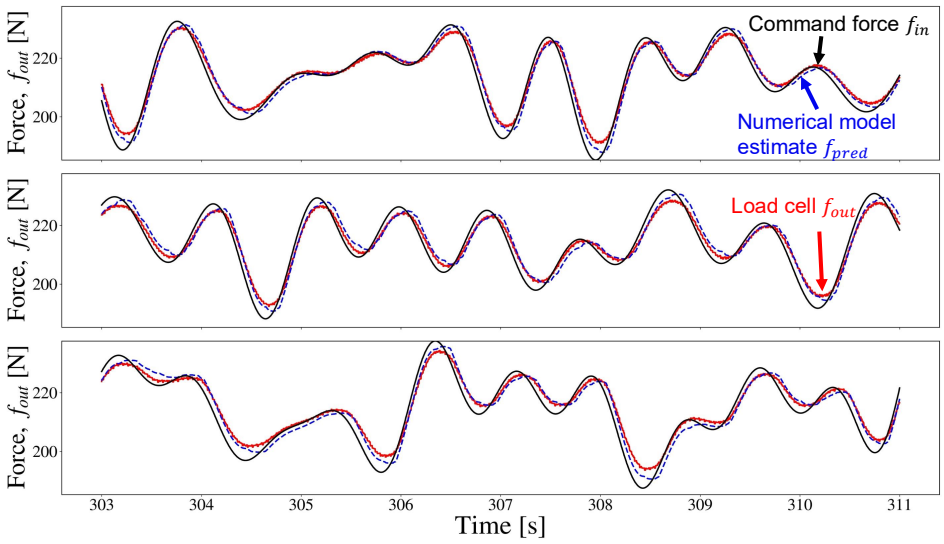

Figure 5: Comparison of command force f_{in}, and numerical model prediction of force estimates f_{pred} against actual force readings from load cell f_{out}. The command force is shown in black, numerical model predictions are shown in the blue dashed line, while the load cell readings are shown in red.

5 Discussion

The linear approximation for the force-deformation relationship in the cable provides an accurate fit, while the numerically simulated model of the motor and cable system exhibits strong predictive capabilities. The numerical model is able to capture approximately correct amplitudes of the force in the load cell and the delay in force transmission due to the cable. The parameters in the numerical model influence the results with varying sensitivities. The constant Coulomb friction term serves to reduce peak amplitudes, while the inertia term models the delay between the command and output force. The velocity-proportional damping term had little effect on the results, likely because the motor velocities were small. The stiffness terms model the amplitude of the force during dynamic loading.

In comparing the numerical model estimates and the experimental data, the discrepancy, particularly at peak amplitudes, can arise due to several reasons (Fig. 5). The current model only accounts for the force-deformation relationship, yet for higher loading rates, the cable force may also have additional rate-dependencies. This may explain the difference between the numerical model and experimental data at higher amplitudes and frequencies, where the stiffness of the cable may be less well approximated. This can be further examined by introducing varying loading rates into the system and using a spring-damper model to approximate the velocity-dependent forces in the cable. Additionally, the experimental setup could have loose connections between the load cell and the cable, resulting in slack conditions during the ramp period and potential geometric nonlinearities. Lastly, a certain amount of friction may have a quadratic dependency with velocity, which is not modeled. The above analysis contributes to strengthening the accuracy of the virtual model, aiding in preliminary analysis and troubleshooting prior to flume testing.

6 Conclusion

This work illustrates the development of a virtual hybrid simulation with a modular, three-loop architecture to analyze the response of deep-water wave energy converters. Experimental data obtained from a simplified bench-test setup at Oregon State University was used to derive a numerical model of the actuation motor and cable system. Nonlinearities in the system were accounted for via constant and damping friction, and springs were used to approximate the force-deformation relationship in the cable and motor after pretension loading. While the numerical model exhibits strong predictive capabilities, discrepancies in higher amplitude/frequency regions highlight the importance of characterization tests to capture system behavior under higher loading rates. The model was more sensitive to the constant friction, which served to reduce peak amplitudes, while the velocity-dependent damping term affected the approximations less. The cable stiffness under dynamic loading were also estimated to be higher than under static loading. Some limita-

tions of this study include using simplified stiffness models of the cable and motor. To address this, future work will involve fine tuning the numerical model of the motor and cable to incorporate geometric nonlinearities and strain-rate dependencies, as well as independent studies to analyze the cable behavior under loading. With the complete virtual model, parametric studies of varying wave loading cases and water depths will also be applied to assess device behavior as a means of early troubleshooting prior to flume testing. The virtual framework presented herein can contribute to designing hybrid simulations that virtually extend the depths of existing wave basins or flumes, facilitating more efficient testing and validation of offshore structures and devices.

Acknowledgments

This work was supported in part by the U.S. Department of Energy under the Applied Research and Development to Support Open-Water Testing at PacWave award (EE0009969). The authors also express their appreciation to the research assistants of O.H. Hinsdale Wave Research Laboratory at Oregon State University. The authors also express their appreciation for support from industry via Maffei Structural Engineering. The findings, opinions, recommendations, and conclusions in this paper are those of the authors alone and do not necessarily reflect the views of others, including the sponsors.

References

[1] Gunnar Mørk et al. “Assessing the Global Wave Energy Potential”. In: vol. 29th International Conference on Ocean, Offshore and Arctic Engineering: Volume 3. International Conference on Offshore Mechanics and Arctic Engineering. June 2010, pp. 447–454. DOI: 10.1115/OMAE2010-20473. eprint: https://asmedigitalcollection.asme.org/OMAE/proceedings-pdf/OMAE2010/49118/447/4588111/447_1.pdf. URL: https://doi.org/10.1115/OMAE2010-20473.

[2] AbuBakr S. Bahaj. “Generating electricity from the oceans”. In: *Renewable and Sustainable Energy Reviews* 15.7 (2011), pp. 3399–3416. ISSN: 1364-0321. DOI: https://doi.org/10.1016/j.rser.2011.04.032. URL: https://www.sciencedirect.com/science/article/pii/S1364032111001900.

[3] B. Buchner, J.E.W. Wichers, and J.J. de Wilde. “Features of the State-of-the-art Deepwater Offshore Basin”. In: vol. All Days. OTC Offshore Technology Conference. May 1999, OTC-10814–MS.

[4] Carl Trygve Stansberg, Harald Ormberg, and Ola Oritsland. “Challenges in Deep Water Experiments: Hybrid Approach”. In: *Journal of Offshore Mechanics and Arctic Engineering* 124.2 (Apr. 2002), pp. 90–96. ISSN: 0892-7219. DOI: 10.1115/1.1464129. eprint: https://asmedigitalcollection.asme.org/offshoremechanics/article-pdf/124/2/90/6839026/90_1.pdf. URL: https://doi.org/10.1115/1.1464129.

[5] Koichi Takanashi et al. “Nonlinear earthquake response analysis of structures by a computer-actuator on-line system”. In: *Bulletin of Earthquake Resistant Structure Research Center* 8 (1975), pp. 1–17.

[6] Stefan A. Vilsen, Thomas Sauder, and Asgeir J. Sørensen. “Real-Time Hybrid Model Testing of Moored Floating Structures Using Nonlinear Finite Element Simulations”. In: *Dynamics of Coupled Structures, Volume 4*. Ed. by Matthew S. Allen, Randall L. Mayes, and Daniel Jean Rixen. Cham: Springer International Publishing, 2017, pp. 79–92.

[7] S.A. Vilsen et al. “Method for Real-Time Hybrid Model Testing of ocean structures: Case study on horizontal mooring systems”. In: *Ocean Engineering* 172 (2019), pp. 46–58. ISSN: 0029-8018. DOI: https://doi.org/10.1016/j.oceaneng.2018.10.042. URL: https://www.sciencedirect.com/science/article/pii/S0029801818320651.

[8] Yusong Cao and Galin Tahchiev. “A Study on an Active Hybrid Decomposed Mooring System for Model Testing in Ocean Basin for Offshore Platforms”. In: vol. Volume 1: Offshore Technology. International Conference on Offshore Mechanics and Arctic Engineering. June 2013, V001T01A080. DOI: 10.1115/OMAE2013-11471. eprint: https://asmedigitalcollection.asme.org/OMAE/proceedings-pdf/OMAE2013/55317/V001T01A080/4428076/v001t01a080-omae2013-11471.pdf. URL: https://doi.org/10.1115/OMAE2013-11471.

[9] Thomas Sauder et al. "Active truncation of slender marine structures: Influence of the control system on fidelity". In: *Applied Ocean Research* 74 (2018), pp. 154–169. ISSN: 0141-1187. DOI: https://doi.org/10.1016/j.apor.2018.02.023. URL: https://www.sciencedirect.com/science/article/pii/S014111871730682X.

[10] Christian E. Silva et al. "Benchmark control problem for real-time hybrid simulation". In: *Mechanical Systems and Signal Processing* 135 (2020), p. 106381. ISSN: 0888-3270. DOI: https://doi.org/10.1016/j.ymssp.2019.106381. URL: https://www.sciencedirect.com/science/article/pii/S0888327019306028.

[11] Gilberto Mosqueda. "Continuous hybrid simulation with geographically distributed substructures". en. ISBN: 9780542252631. Ph.D. Berkeley, California, USA: University of California, Berkeley, 2003. URL: https://www.proquest.com/docview/305344082/abstract/4DC0CEFEE30648C1PQ/1 (visited on 08/09/2023).

[12] Matthew Hall and Andrew Goupee. "Validation of a lumped-mass mooring line model with DeepCwind semisubmersible model test data". In: *Ocean Engineering* 104 (2015), pp. 590–603. ISSN: 0029-8018. DOI: https://doi.org/10.1016/j.oceaneng.2015.05.035. URL: https://www.sciencedirect.com/science/article/pii/S0029801815002279.

[13] Kelley Ruehl et al. *WEC-Sim/WEC-Sim: v6.1.2*. Version v6.1.2. Jan. 2025. DOI: 10.5281/zenodo.14648966. URL: https://doi.org/10.5281/zenodo.14648966.

[14] Raza Ali, Moira Meek, and Bryson Robertson. "Submerged wave energy converter dynamics and the impact of PTO-mooring configuration on power performance". In: *Renewable Energy* (2025), p. 122525. ISSN: 0960-1481. DOI: https://doi.org/10.1016/j.renene.2025.122525. URL: https://www.sciencedirect.com/science/article/pii/S0960148125001879.

[15] Senu Sirnivas et al. "Coupled Mooring Analyses for the WEC-Sim Wave Energy Converter Design Tool: Preprint". In: National Renewable Energy Lab. (NREL), Golden, CO (United States). July 2016. DOI: 10.1115/OMAE2016-54789. URL: https://www.osti.gov/biblio/1263540.

[16] Samson Rope Technologies. *AmSteel®-Blue Rope*. URL: https://www.samsonrope.com/mooring/amsteel--blue.

[17] Sensing Systems Corporation. *Underwater Load Cells*. 2025. URL: https://sensing-systems.com/underwater-load-cells/.

[18] Akribis Systems. *ADR-B Series Iron Core Rotary Motor*. 2025. URL: https://akribis-sys.com/products/rotary-stages/adr-b-series/.

[19] Andreas H. Schellenberg, Stephen A. Mahin, and Gregory L. Fenves. *Advanced implementation of hybrid simulation*. en. Tech. rep. PEER 2009/104. Berkeley, California, USA: Pacific Earthquake Engineering Research Center, 2009.

[20] *Streamlined Loads Analysis of Floating Wind Turbines With Fiber Rope Mooring Lines*. Vol. ASME 2023 5th International Offshore Wind Technical Conference. International Conference on Offshore Mechanics and Arctic Engineering. Dec. 2023, V001T01A029. DOI: 10.1115/IOWTC2023-119524. eprint: https://asmedigitalcollection.asme.org/OMAE/proceedings-pdf/IOWTC2023/87578/V001T01A029/7234396/v001t01a029-iowtc2023-119524.pdf. URL: https://doi.org/10.1115/IOWTC2023-119524.

[21] American Bureau of Shipping. *The Application of Fiber Rope for Offshore Mooring*. Technical Report. Houston, Texas: American Bureau of Shipping, June 2021.